Phase diagram of uranium from *ab initio* calculations and machine learning

Ivan A. Kruglov,[1,2,*] Alexey Yanilkin,[1,2] Artem R. Oganov,[3,2,1] and Pavel Korotaev[1,4]

[1]*Dukhov Research Institute of Automatics (VNIIA), Moscow 127055, Russian Federation*

[2]*Moscow Institute of Physics and Technology, Dolgoprudny 141700, Russian Federation*

[3]*Skolkovo Institute of Science and Technology, Skolkovo Innovation Center, Moscow 143026, Russian Federation*

[4]*Material Modeling and Development Laboratory, NUST MISiS, Moscow 119991, Russian Federation*

(Received 7 May 2019; revised manuscript received 17 October 2019; published 12 November 2019)

Experimental studies of materials at extreme conditions are challenging, and as a consequence, *P-T* phase diagrams are still unknown for many elements and materials. In this work, we present the *P-T* phase diagram of uranium calculated up to extreme conditions. First, we searched for possible crystal structures using the evolutionary algorithm USPEX. Their free energies were then calculated using thermodynamic integration (TI) and temperature-dependent effective potential techniques. TI was performed using molecular dynamics, employing a machine learning (ML) force field trained on energies and forces from density-functional calculations at the generalized gradient approximation level. The prediction error of the ML force field for the energy was less than 10 meV/atom. Using thermodynamic perturbation theory (including first and second order corrections), from the free energies of the ML force field, we obtained free energies and phase diagram at the level of quality of the underlying density-functional calculations at pressures up to 800 GPa and temperatures up to 16 000 K.

DOI: 10.1103/PhysRevB.100.174104

I. INTRODUCTION

Uranium is one of the most important elements in nuclear industry, yet its phase diagram at extreme conditions remains unknown. It has several low-temperature phases, including the orthorhombic α phase (stable at normal conditions), high-temperature tetragonal β phase, body-centered cubic (*bcc*) γ phase [1] and high-pressure *bct* γ' phase. The difference between two tetragonal phases is that γ'-U has *I4/mmm* space group with $Z = 2$, while β-U has uncertain space group ($P4_2/mnm$, $P4_2nm$, or $P\bar{4}n2$) with $Z \sim 30$. It was found that at ambient pressure α phase transforms into the β phase at 940 K and then into the γ phase at 1050 K. As pressure increases, the β phase rapidly disappears from the phase diagram in a triple point at ~3 GPa and ~1000 K[2]. At temperatures below 50 K, α-U experiences a sequence of two first-order and one second-order phase transitions, with the charge density wave formation and superconducting states arising in succession [2–5]. High-pressure phase transitions were experimentally investigated in a laser-heated diamond anvil cell at pressures up to 100 GPa and temperatures 4500 K [6–9]. We will use these data for comparison and will extend the phase diagram to much higher pressures and temperatures.

Phase diagrams can be studied using different theoretical techniques. Quantum-mechanical approaches, such as density functional theory (DFT), are often applied, but become expensive at nonzero temperatures. For example, DFT was used to study structural properties in the equilibrium α-U phase [10–13], its elastic properties [13–15], and compression stability [16,17]. It was shown that the α phase transforms into the *bct* γ' phase at 285 GPa, while γ-U is 0.1–0.2 eV/atom higher in enthalpy than the *bct* phase up to 500 GPa with a possible transition from γ'-U to γ-U at 2.3 TPa [16]. To check whether there are other low-enthalpy phases that might have stability fields on the *P-T* phase diagram, we can use global optimization techniques, such as the evolutionary algorithm USPEX [18–20]. Investigating phase stability at high temperatures is trickier, as it requires that thermal contribution to the free energy be taken into account. High-temperature phase stability can be studied using a variety of approaches, including the finite-displacements method [21–23], self-consistent *ab initio* lattice dynamics (SCAILD) [24], temperature-dependent effective potential (TDEP) [25,26], and thermodynamic integration (TI) [27–30] techniques. Recently, the TDEP technique was used in combination with *ab initio* molecular dynamics (AIMD) to explore the phase diagram of uranium at pressures up to 100 GPa and temperatures up to 2000 K [31]. The study did not only reveal strong anharmonic effects in uranium, but also showed that when anharmonicity is properly included, the theoretical α-γ equilibrium line on the phase diagram agrees well with the experiment from Ref. [6].

The SCAILD and TDEP techniques are approximate, whereas the TI method is exact, although it requires a large supercell and long simulation times and, therefore, is expensive. Much cheaper calculations can be done using classical molecular dynamics based on force fields, for example, the embedded atom model (EAM) [32] and modified embedded atom model [33] potentials. The EAM potential from Ref. [34] provided a fairly good description of the α-γ transition in uranium at zero pressure. Another EAM potential [35] developed using the force matching technique was quite accurate in reproducing lattice parameters and bulk modulus of α-U and the melting curve of U at pressures up to 80 GPa. Other force fields for U exist [36–38], and were used for predicting

*Corresponding author: ivan.kruglov@phystech.edu

the melting curve at pressures up to 800 GPa [38]. However, the α-γ' (*bct*) and γ'-γ equilibrium lines remained unknown. Generally, the use of force fields can lead to significant errors. A possible solution is to parameterize the force field for each thermodynamic state independently so that the DFT data are reproduced for that state as accurately as possible and the errors in the free energy are minimal. This strategy was adopted in Refs. [39–41] to calculate the free energy of copper with the EAM potential, and aluminum and iron with the inverse-power potential.

Recently, we used machine learning (ML) to develop accurate force fields [42]. Various ML-based interatomic potentials are now used extensively and their training on data from *ab initio* molecular dynamics simulation is becoming a common strategy. Neural network potentials were developed [43,44] and applied to sodium [45,46], silicon [47], water [48], and zinc oxide [49]. The Gaussian approximation potential (GAP) based on the bispectrum feature vector and Gaussian regression was constructed and applied to many problems [50–53]. The moment tensor potential approach (MTP) [54–57] is another promising approach, as it offers higher efficiency than GAP, while having the same accuracy [58]. A comparison between different methods can be found in Ref. [59].

In this work, we applied a two-step strategy to study the phase diagram of uranium up to 800 GPa and 16 000 K. First, we found plausible candidate crystal structures at pressures up to 800 GPa. Then, their free energies were obtained as a function of temperature using two approaches: rigorous TI method and less accurate (since it does not account for the full anharmonic contribution to the free energy) TDEP approach, and we compare results of these methods. For the melting line calculation we used the modified Z method [60].

II. COMPUTATIONAL METHODOLOGY

We conducted searches for lowest-enthalpy structures of uranium with a variable number of atoms using evolutionary algorithm USPEX [18–20] at zero temperature and pressures of up to 800 GPa. The first-generation crystal structures were created using random symmetric [19] and random topological [61] structure generators, and each subsequent generation comprised 30% random structures and 70% structures created using heredity, softmutation and lattice mutation operators. We explored systems with variable number of atoms in the primitive unit cell (from 8 to 16), at pressures 0, 100, 200, and 300 GPa. The structure that had the lowest enthalpy in 30 successive generations was considered the most stable one. Structure relaxations and energy calculations were performed using (DFT within Perdew-Burke-Ernzerhof [62] functional, as implemented in the VASP code [63–65]. The projector-augmented wave (PAW) [66] method was used to describe core electrons and their interaction with valence electrons; we used PAW potentials with 14 valence electrons and 2.8 Å core radius (at the highest pressure explored, 800 GPa, the overlap between core regions was 3.32 Å). The plane wave kinetic energy cutoff was set at 500 eV and Γ-centered k-point meshes with the resolution of $2\pi \times 0.05\,\text{Å}^{-1}$ were used for sampling the Brillouin zone. The phase diagram was built based on the free energies obtained using the TI method. TI was performed along the nonequilibrium trajectory of the Frenkel-Ladd path [67] from the actual system (i.e., the ML force field) to the reference potential and back, as was described in Ref. [68]. Calculating the absolute value of the free energy requires a reference potential with known free energy, such as the Einstein crystal, which is suitable for the solid state. This strategy is very similar to that published in Refs. [39–41]. The melting line was calculated using the modified Z method [60] from a solid-liquid coexistence state. For this, we used a simulation box, the length of which in one direction is much larger in comparison with the others. The initial temperature was set approximately two times the expected melting point. If the initial energy was high enough, then in the *NVE* ensemble the simulated system evolved into the steady solid-liquid coexistence state. Its average temperature equals to the melting temperature of the solid.

The ML force field was trained on results (configurations, energies, forces) of *ab initio* MD calculations, which were performed at temperatures from 1000 to 3000 K for α-U, from 1000 to 5000 K for γ'-U and from 1000 to 15 000 K for γ-U. The ML force field was formulated following Ref. [69]. The feature vector, characterizing each configuration, is defined as

$$\boldsymbol{X_E} = \sum_{i=1}^{N_{at}} \sum_{j=1}^{N^i_{\text{neigh}}} \exp\left[-\left(\frac{r_{ij}}{r_{\text{cut}}(l)}\right)^{p(l)}\right],\ l = 1 \ldots k, \quad (1)$$

where N_{at} is the number of atoms in the unit cell, N^i_{neigh} is the number of neighboring atoms of the i^{th} atom, r_{cut} and p are the constants that must be chosen optimally, and $r_{ij} = |\overrightarrow{r_{ij}}|$. The length of the feature vector is equal to the number of (r_{cut}, p) pairs. Following our recent work [42], we used linear regression with regularization as the ML algorithm, which means that the energy is a linear function of the feature vector and, therefore, the forces are derivatives of the energy with respect to atomic positions (with the minus sign). In this case the energy is determined as

$$E = \Theta X_E + \Theta_0, \quad (2)$$

where Θ denotes coefficients of linear regression. Thus, the force on atom i in the x direction (equations being the same for the y and z directions) is defined as

$$f_{x,i} = -\frac{\partial E}{\partial x_i} = -\Theta \frac{\partial X_E}{\partial x_i} = \Theta X_f. \quad (3)$$

To find the parameters of linear regression, we solve $E = \Theta X_E + \Theta_0$ and $f = \Theta X_f$ equations with respect to Θ:

$$\Theta = \left(X_E^T X_E\right)^{-1} E,\ \Theta = \left(X_f^T X_f\right)^{-1} f. \quad (4)$$

Here, a bias Θ_0 is included in Θ. To satisfy Eqs. (2) and (3), we add rows of ones and zeros to the X_E and X_f matrices, respectively. The algorithm is trained simultaneously on energies E and forces f. After finding Θ, we can apply Eqs. (2) and (3) to calculate the energies and forces on atoms in a new structure. We implemented this potential in the LAMMPS [70] code using the LAMMPS domain decomposition for parallelization.

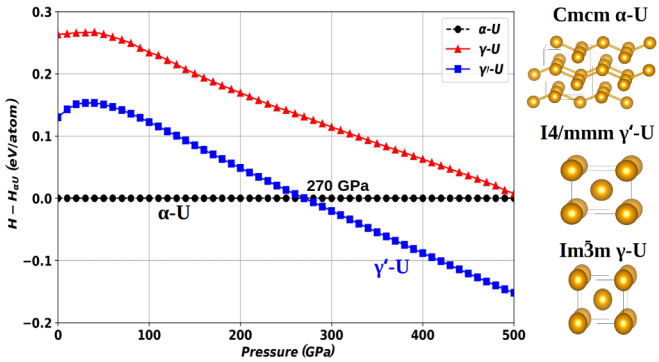

FIG. 1. Enthalpies of γ'-U and γ-U (relative to α-U) as a function of pressure (left). Crystal structures of these phases are shown on the right.

III. RESULTS

A. Stability of uranium phases at 0 K

First, we looked at stability of uranium phases at zero Kelvin. We conducted global optimization, searching for the most stable (and low-enthalpy metastable) uranium phases using USPEX. This is a more rigorous approach than what was used in previous works (e.g., Ref. [16]), where calculations there were limited to comparing enthalpies of known uranium phases and the most common crystal structure types (*fcc* and *hcp*). USPEX makes no assumptions about possible crystal structures and is capable of predicting completely unexpected and even counterintuitive phases [71–75]. In our USPEX calculations we found previously known *Cmcm* α-U and *P4/mmm* γ'-U to be the most stable structures, with the transition pressure of 270 GPa (Fig. 1). Accounting for zero-point energy shifts α-U $\rightarrow$ γ'-U transition pressure at zero temperature to 265 GPa (See Supplemental Material Fig. S1 [76]). According to DFT calculations, *bcc*-structured (space group $Im\bar{3}m$) γ-U is always $\sim$0.1−0.15 eV/atom higher in enthalpy than the γ'-U phase (yet γ-U is known to be stable at higher temperatures[2]), so any new phase which is lower in enthalpy than γ-U could be stable at high temperature. We found seven phases that satisfy this condition (see Figs. S2–S3). Hereinafter we will discuss their potential stability in the full *P-T* space explored here.

B. Accuracy of ML interatomic potential for uranium phases

As the next step, we computed free energies of different phases of uranium and built the phase diagram. Free energy was calculated by applying the TI technique during MD simulation with the ML force field. To reach the highest possible accuracy at a specific density and temperature, we trained a new ML potential at each temperature and density. We emphasize that at high temperatures, it is important to include the electronic contribution to thermodynamic properties; we did this by training ML force fields on Mermin's [77] DFT free energy, which includes electronic entropy computed via Fermi-Dirac smeared occupancies of the electronic states.

A training set for each ML potential consisted of 20% structures chosen randomly from a 5-ps AIMD trajectory. We used 3 × 3 × 3 supercells for γ and γ' and 3 × 2 × 2 for α phase. The k-point mesh was 2 × 2 × 2 in all the calculations. We used 11 equally distributed (r_{cut}, p) pairs taken from [1,5] and [3,1] intervals, respectively (for more details on the procedure, see Ref. [42].) Earlier, we demonstrated [42] that this leads to lower errors for the forces than with traditional force fields. The accuracy of the free energy calculation depends on how accurately it reproduces the potential energy surface. Figure 2 shows the root-mean-squared error (RMSE) for the energies for different U phases at different conditions, and one can see that the lowest and highest errors are 2 and 14 meV/atom, respectively, while the average error is below 10 meV/atom. With a force field of such quality, we can compute reasonably accurate free energies, eliminating the remaining errors later by the use of thermodynamic perturbation theory.

C. Free energy calculation and $P-T$ phase diagram

To begin with, new uranium phases found by USPEX (from Fig. S2 [76]) were considered at $\rho = 29.28\,\text{g/cm}^3$ and $T = 3000\,\text{K}$. We chose to check such a high temperature because all the new structures are metastable at zero Kelvin, and the only possibility for them to become stable is due to entropic stabilization at high temperatures. First we performed a 10-ps MD run in the *NVE* ensemble (at $T = 3000\,\text{K}$) with a 1000-atom supercell, using the ML interatomic potential. We found the same behavior for all newly predicted structures, and we discuss here *Cmcm*-U as an example. During MD simulation in the *NVE* ensemble, this structure relaxed to a new *bct*-U phase ("bct2") differing from γ'-U in that it had smaller lattice parameters a and b as compared to c. In order to check the stability of the "bct2"-U phase, a MD simulation in the *NPT* ensemble at 3000 K and corresponding pressure is needed. However, our ML force field was not trained on stresses, so we used a MTP force field [58]. It assumes that energy linearly depends on the basis functions which are in turn functions of atomic neighborhoods. The basis functions satisfy all symmetries such as rotation invariance and invariance with respect to permutation of atoms of the same type and have explicit expressions for calculation of the forces and stresses. The number of basis functions is chosen as a compromise between the accuracy and computational efficiency of the potential. In this work we used 100 basis functions. Using MTP potentials the "bct2"-U phase relaxed to the previously known γ-U. γ-U does not correspond to an energy minimum, is anharmonically stabilized and covers a wide basin on the energy landscape. Note that here we used the MTP force field for *NPT* molecular dynamics, but not for free energy calculations, as it often fails during thermodynamic integration, because phase space changes significantly while integrating to Einstein crystal and backwards. ML potential, presented in this work, is based on smooth exponential functions, appears to behave better in rare situations where extrapolation is needed, and, therefore, it was used for free energy calculations.

Having selected the most relevant structures, we computed their free energies. The spring constants of Einstein crystals used for TI were selected for different phases and densities in order to minimize the free energy difference from the reference system. This allows using the shortest integration

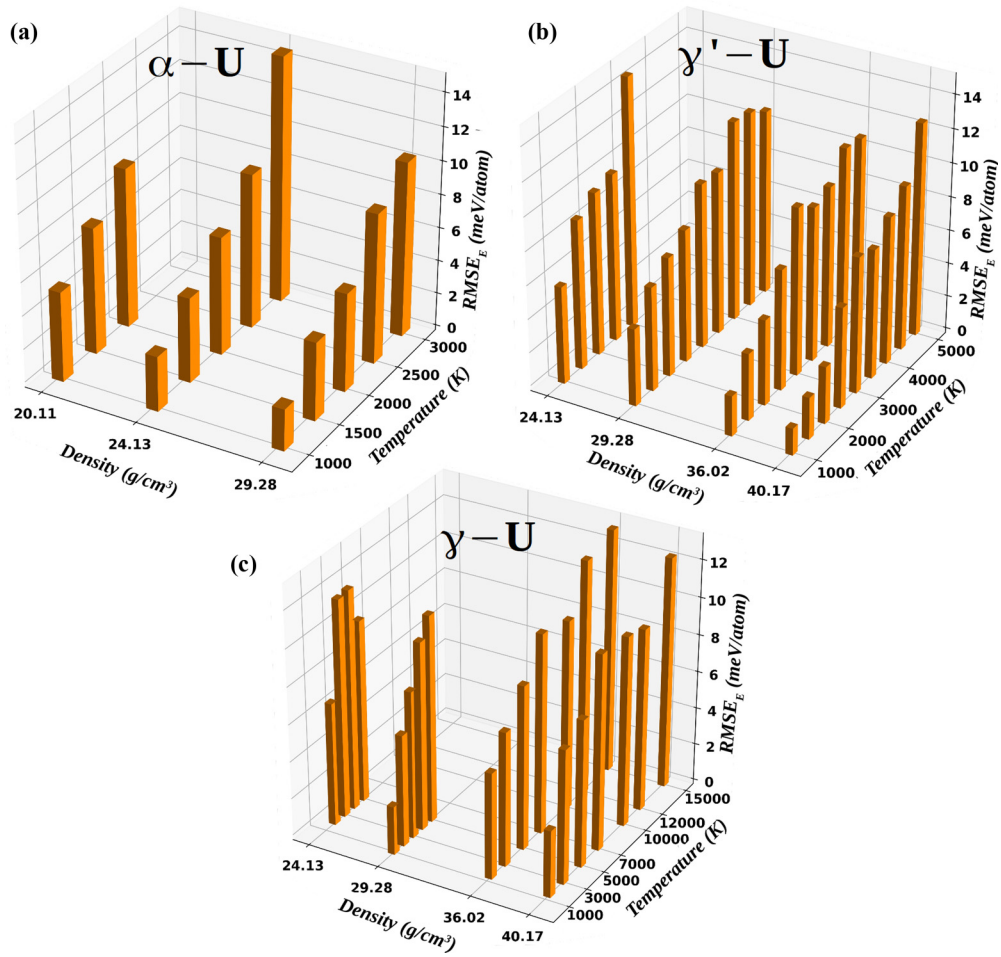

FIG. 2. Root-mean-squared errors (RMSE) shown as histograms of the ML force fields for (a) α, (b) γ', and (c) γ-U phases at different densities and temperatures

times between two potentials and relatively small supercells. These spring constants are given in Table S2.

Two points should be mentioned. First, an increase in density produces an increase in the spring constant for all the phases. Second, the close-packed structure, α uranium, has the highest spring constant, whereas the anharmonically stabilized γ phase has the lowest one, the γ' phase being in between. With these spring constants, typical supercell size (2000 atoms) and TI time (20 ps), we computed free energies with precision better than 1 meV/atom.

These free energies, corresponding to a ML force field, were then used to obtain full DFT values of the free energy with corrections from thermodynamic perturbation theory [78]. Given a reasonably good ML force field (which we clearly do have), one can obtain free energies virtually indistinguishable from full DFT free energies using thermodynamic perturbation theory, which to second order gives the following Helmholtz free energy difference (per atom) between the *ab initio* system and the system described by the ML force field [39,41]:

$$\Delta F \simeq \frac{1}{N_{at}}\left[\langle U - U_0\rangle_0 - \frac{1}{2k_bT}\langle[U - U_0 - \langle U - U_0\rangle]^2\rangle_0\right], \tag{5}$$

where U is the total energy computed with our force field, U_0 is the reference DFT energy, and N_{at} is the number of atoms. As it turns out, corrections due to Eq. (5) are mild, shifting phase transition temperatures by less than 150 K (Fig. 3).

Helmholtz free energies of α, γ', and γ phases, computed as a function of temperature at a fixed densities are shown in Fig. 3. Each $F(T)$ line was fitted using the least squares method to given values of free energies (marked with disk and triangle in Fig. 3). This brings an additional error to transition temperature estimation of about 50 K. At each density, temperature of phase equilibrium corresponds to crossing of the $F(T)$ lines, and phase equilibrium pressure is obtained by averaging pressures of the two phases (at given V and T) [79,80]: $P = \frac{P_I + P_{II}}{2}$; the maximum error of this estimate is $\frac{P_I - P_{II}}{2}$ (here, only a few GPa).

The importance of anharmonicity is seen in Fig. 3(a), which shows the free energy of *bct*-U phase obtained using the quasiharmonic approximation (F_{harm}) and fully anharmonic free energies of all phases obtained using TI. It is clear from Fig. 3(a) that quasiharmonic and fully anharmonic free energies are very different, which is indicative of strong anharmonic effects.

Figure 3 shows that at the density of 29.3 g/cm^3, α-U remains stable at temperatures up to 1700 K and then transforms

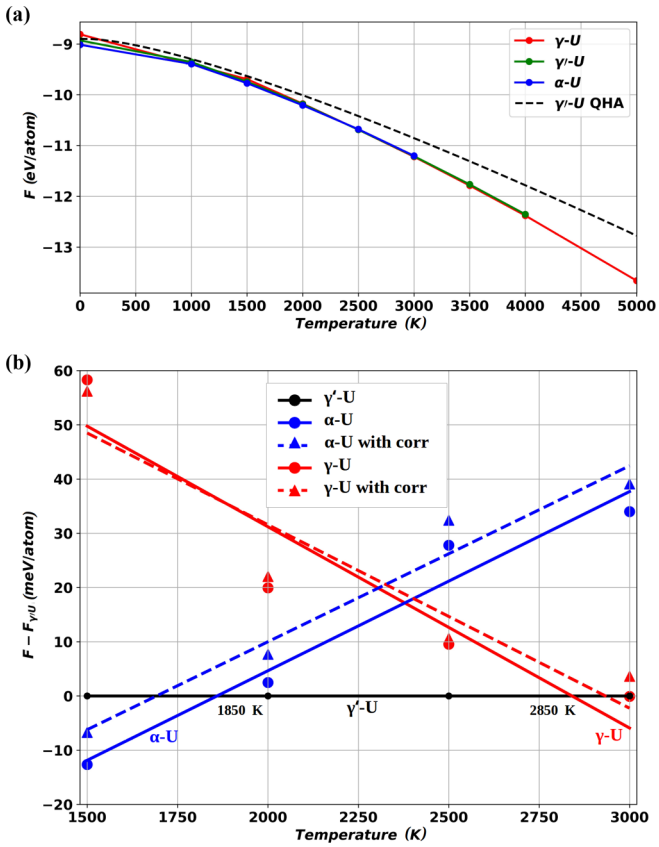

FIG. 3. Free energies of uranium phases as a function of temperature at the density of 29.3 g/cm^3: (a) fully anharmonic free energies and quasiharmonic free energy of γ'-U, all based on our ML force field, and (b) fully anharmonic free energies relative to γ'-U, obtained using our ML force field and at DFT level of theory (using thermodynamic perturbation theory).

to gamma′-U, which then transforms to gamma-U at 2900 K (with thermodynamic perturbation theory corrections taken into account). Then for a given density and temperature (in this case 1700 K and 29.3 g/cm^3) using the $P(V,T)$ function we calculated the corresponding pressure (162 GPa in this case). In order to verify the obtained results, we also calculated free energies of different phases of uranium using TDEP fitted directly to the AIMD data. The free energies calculated with different methods are compared in Fig. S4 [76], where one can see a minor difference between the values of the free energy, becoming greater at higher temperatures. The temperature of the phase transition from α- to γ' phase calculated using TDEP at $\rho = 29.3\,\mathrm{g/cm^3}$ is equal to 2000 K, which shows semiquantitative agreement between two methods. As TI is a more rigorous way of calculating free energies, all results reported here are based only on TI.

Computing free energies and P-T points of phase equilibria, we built the phase diagram of uranium (Fig. 4). A more detailed phase diagram (with plotted calculated transition and melting points) is shown in supplementary Fig. S6 [76]. We found that α-U transforms to γ'-U at 64 GPa and 1500 K, and then γ'-U to γ-U at 2000 K. In Ref. [31] the authors did not consider γ'-U phase and showed that α-U transforms to γ-U at almost the same conditions (∼60 GPa and 1500 K). With

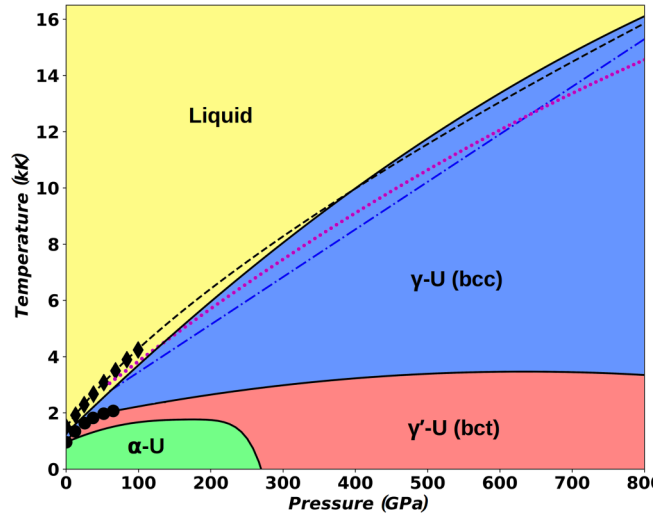

FIG. 4. Phase diagram of uranium. Black diamonds and circles denote experimental data from Ref. [6]. Solid black lines correspond to our computed phase boundaries. Dashed black line is the extrapolated experimental melting line using Simon-Glatzel law [81], dotted magenta and dashed (with dots) blue lines are melting lines from Ref. [38].

rising temperature γ'-U transforms to *bcc* γ-U, which remains stable up to the melting temperature. TDEP calculations show qualitatively similar results.

To calculate the melting curve of uranium, we used the modified Z method [60]. The system ($4 \times 4 \times 100$ *bcc*-U supercell) was simulated at a fixed density in the *NVE* ensemble. Initially the temperature was set approximately two times higher than estimated melting point. Shortly after the start, temperature decreased to some constant value, and then melting happened. Calculated melting temperatures at different densities are shown in Table I. For comparison, the experimental melting line was extrapolated to high P-T conditions using Simon-Glatzel law [81] ($T_S(P) = T_0(1 + aP)^c$) with parameters taken from Ref. [38].

Our final results for the melting curve also included corrections from thermodynamic perturbation theory. Free energy correction ΔF will induce a shift ΔT in the melting temperature, such that $\Delta T = \frac{\Delta F}{\Delta S_m}$, where ΔS_m is the entropy of melting. The latter can be calculated from the Clausius-Clapeyron relation: $\Delta S_m = \frac{dP}{dT}\Delta V_m$, where $\frac{dP}{dT}$ is the slope of the melting curve, and ΔV_m can be calculated from the two-phase system formed during melting temperature calculation (all values are presented in Table I). As we can see from Table I, the melting curve is shifted only slightly due

TABLE I. Melting properties of U at different densities.

Density (g/cm^3)	24.1	29.3	36.0	40.2
T_{melt} (K) (ML)	2822	6232	11822	16052
ΔV_m(Å^3)	0.27	0.23	0.19	0.13
$\Delta S_m(k_B)$	0.84	0.81	0.8	0.8
ΔT (K)	−26	18	−13	−20
$T^{\mathrm{corr}}{}_{\mathrm{melt}}$ (K) (DFT)	2796	6250	11809	16032

to thermodynamic perturbation theory corrections. The final melting curve of γ-U is in good agreement with experimental data (Fig. 4, black diamonds), but is about 1500 K higher than previous results obtained using DFT and EAM potentials [38] (dotted magenta and dashed (with dots) blue lines in Fig. 4, respectively). At the pressure of 800 GPa, uranium melts at almost 16 000 K.

IV. CONCLUSIONS

In this work, we present the *P-T* phase diagram of uranium computed to pressures up to 800 GPa and temperatures up to 16000 K. To do this, we first constructed an accurate (RMSE within 10 meV/atom) machine learning force field. This cheap and accurate machine learning force field allowed us to study large systems, perform long molecular dynamics simulations, and obtain accurate free energies. First, free energies of different phases were calculated to zeroth-order approximation based on machine learning force fields and using thermodynamic integration from the Einstein crystal. Fully anharmonic *ab initio* free energies were obtained by adding to these free energies first- and second-order corrections from thermodynamic perturbation theory. Such corrections were also applied to the melting curve. As a result, we obtained an *ab initio* quality phase diagram of uranium up to ultrahigh pressures and temperatures.

The phase diagram shows that the only phases with wide stability field at conditions up to 800 GPa and 16000 K are the previously known α-U, γ-U, and γ'-U. α-U is stable up to 270 GPa and 1500 K. Then, with rising temperature, it transforms first to γ'-U and then to γ-U. The presented approach is general and enables building *P-T* phase diagrams of any element or (with some modification) compound. For example, phase diagrams of other actinides with a much wider variety of different phases can be studied.

ACKNOWLEDGMENTS

This work was supported by a grant from the Russian Foundation for Basic Research 18-32-00622. We also thank O. Sergeev for integration of the ML potential in LAMMPS code.

[1] D. A. Young, *Phase Diagrams of the Elements* (University of California Press, Berkeley, 1991).
[2] E. S. Fisher and H. J. McSkimin, Phys. Rev. **124**, 67 (1961).
[3] E. S. Fisher and D. Dever, Phys. Rev. **170**, 607 (1968).
[4] T. F. Smith and E. S. Fisher, J. Low Temp. Phys. **12**, 631 (1973).
[5] M. O. Steinitz, C. E. Burleson, and J. A. Marcus, J. Appl. Phys. **41**, 5057 (1970).
[6] C.-S. Yoo, H. Cynn, and P. Söderlind, Phys. Rev. B **57**, 10359 (1998).
[7] J. Akella, G. S. Smith, R. Grover, Y. Wu, and S. Martin, High Press. Res. **2**, 295 (1990).
[8] J. Akella, S. Weir, J. M. Wills, and P. Söderlind, J. Phys. Condens. Matter **9**, L549 (1997).
[9] T. Le Bihan, S. Heathman, M. Idiri, G. H. Lander, J. M. Wills, A. C. Lawson, and A. Lindbaum, Phys. Rev. B **67**, 134102 (2003).
[10] J. P. Crocombette, F. Jollet, L. Thien Nga, and T. Petit, Phys. Rev. B **64**, 104107 (2001).
[11] P. Söderlind, Phys. Rev. B **66**, 085113 (2002).
[12] C. D. Taylor, Phys. Rev. B **77**, 094119 (2008).
[13] B. Beeler, C. Deo, M. Baskes, and M. Okuniewski, J. Nucl. Mater. **433**, 143 (2013).
[14] A. Dewaele, J. Bouchet, F. Occelli, M. Hanfland, and G. Garbarino, Phys. Rev. B **88**, 134202 (2013).
[15] J. H. Li, Q. B. Ren, C. H. Lu, L. Lu, Y. Dai, and B. X. Liu, J. Alloys Compd. **516**, 139 (2012).
[16] S. Adak, H. Nakotte, P. F. de Châtel, and B. Kiefer, Phys. B **406**, 3342 (2011).
[17] M. Pénicaud, J. Phys.: Condens. Matter **14**, 3575 (2002).
[18] C. W. Glass, A. R. Oganov, and N. Hansen, Comput. Phys. Commun. **175**, 713 (2006).
[19] A. O. Lyakhov, A. R. Oganov, H. T. Stokes, and Q. Zhu, Comput. Phys. Commun. **184**, 1172 (2013).
[20] A. R. Oganov, A. O. Lyakhov, and M. Valle, Acc. Chem. Res. **44**, 227 (2011).
[21] A. Togo and I. Tanaka, Scr. Mater. **108**, 1 (2015).
[22] G. Grimvall, B. Magyari-Köpe, V. Ozoliņš, and K. A. Persson, Rev. Mod. Phys. **84**, 945 (2012).
[23] B. Fultz, Prog. Mater. Sci. **55**, 247 (2010).
[24] P. Souvatzis, O. Eriksson, M. I. Katsnelson, and S. P. Rudin, Comput. Mater. Sci. **44**, 888 (2009).
[25] O. Hellman, I. A. Abrikosov, and S. I. Simak, Phys. Rev. B **84**, 180301(R) (2011).
[26] O. Hellman, P. Steneteg, I. A. Abrikosov, and S. I. Simak, Phys. Rev. B **87**, 104111 (2013).
[27] T. P. Straatsma and H. J. C. Berendsen, J. Chem. Phys. **89**, 5876 (1988).
[28] T. P. Straatsma and J. A. McCammon, J. Chem. Phys. **95**, 1175 (1991).
[29] M. J. Mitchell and J. A. McCammon, J. Comput. Chem. **12**, 271 (1991).
[30] G. Hummer, J. Chem. Phys. **114**, 7330 (2001).
[31] J. Bouchet and F. Bottin, Phys. Rev. B **95**, 054113 (2017).
[32] M. S. Daw and M. I. Baskes, Phys. Rev. B **29**, 6443 (1984).
[33] M. I. Baskes, Phys. Rev. B **46**, 2727 (1992).
[34] M. I. Pascuet, G. Bonny, and J. R. Fernández, J. Nucl. Mater. **424**, 158 (2012).
[35] D. E. Smirnova, S. V Starikov, and V. V Stegailov, J. Phys.: Condens. Matter **24**, 015702 (2012).
[36] D. E. Smirnova, A. Y. Kuksin, S. V Starikov, V. V Stegailov, Z. Insepov, J. Rest, and A. M. Yacout, Model. Simul. Mater. Sci. Eng. **21**, 035011 (2013).
[37] D. E. Smirnova, A. Y. Kuksin, and S. V. Starikov, J. Nucl. Mater. **458**, 304 (2015).
[38] K. P. Migdal, P. A. Pokatashkin, and A. V. Yanilkin, High Temp. **55**, 711 (2017).
[39] L. Vočadlo and D. Alfè, Phys. Rev. B **65**, 214105 (2002).
[40] L. Vočadlo, D. Alfè, G. D. Price, and M. J. Gillan, J. Chem. Phys. **120**, 2872 (2004).

[41] D. Alfè, G. D. Price, and M. J. Gillan, Phys. Rev. B **65**, 165118 (2002).
[42] I. Kruglov, O. Sergeev, A. Yanilkin, and A. R. Oganov, Sci. Rep. **7**, 8512 (2017).
[43] J. Behler and M. Parrinello, Phys. Rev. Lett. **98**, 146401 (2007).
[44] J. Behler, J. Phys.: Condens. Matter **26**, 183001 (2014).
[45] H. Eshet, R. Z. Khaliullin, T. D. Kühne, J. Behler, and M. Parrinello, Phys. Rev. B **81**, 184107 (2010).
[46] H. Eshet, R. Z. Khaliullin, T. D. Kühne, J. Behler, and M. Parrinello, Phys. Rev. Lett. **108**, 115701 (2012).
[47] J. Behler, R. Martoňák, D. Donadio, and M. Parrinello, Phys. Rev. Lett. **100**, 185501 (2008).
[48] T. Morawietz and J. Behler, J. Phys. Chem. A **117**, 7356 (2013).
[49] N. Artrith, T. Morawietz, and J. Behler, Phys. Rev. B **83**, 153101 (2011).
[50] A. P. Bartók, M. C. Payne, R. Kondor, and G. Csányi, Phys. Rev. Lett. **104**, 136403 (2010).
[51] W. J. Szlachta, A. P. Bartók, and G. Csányi, Phys. Rev. B **90**, 104108 (2014).
[52] A. P. Bartók, M. J. Gillan, F. R. Manby, and G. Csányi, Phys. Rev. B **88**, 054104 (2013).
[53] V. L. Deringer and G. Csányi, Phys. Rev. B **95**, 094203 (2017).
[54] R. Ramakrishnan, P. O. Dral, M. Rupp, and O. A. von Lilienfeld, J. Chem. Theory Comput. **11**, 2087 (2015).
[55] V. Botu and R. Ramprasad, Int. J. Quantum Chem. **115**, 1074 (2015).
[56] K. Yao, J. E. Herr, and J. Parkhill, J. Chem. Phys. **146**, 014106 (2017).
[57] K. B. Lipkowitz and D. B. Boyd, *Reviews in Computational Chemistry* (Wiley, Hoboken, NJ, 2007).
[58] A. V. Shapeev, Multiscale Model. Simul. **14**, 1153 (2016).
[59] Y. Zuo, C. Chen, X. Li, Z. Deng, Y. Chen, J. Behler, G. Csányi, A. V. Shapeev, A. P. Thompson, M. A. Wood, and S. P. Ong, arXiv:1906.08888.
[60] S. Wang, G. Zhang, H. Liu, and H. Song, J. Chem. Phys. **138**, 134101 (2013).
[61] P. V. Bushlanov, V. A. Blatov, and A. R. Oganov, Comput. Phys. Commun. **236**, 1 (2019).
[62] J. P. Perdew, K. Burke, and M. Ernzerhof, Phys. Rev. Lett. **77**, 3865 (1996).
[63] G. Kresse and J. Hafner, Phys. Rev. B **47**, 558 (1993).
[64] G. Kresse and J. Hafner, Phys. Rev. B **49**, 14251 (1994).
[65] G. Kresse and J. Furthmüller, Phys. Rev. B **54**, 11169 (1996).
[66] G. Kresse and D. Joubert, Phys. Rev. B **59**, 1758 (1999).
[67] D. Frenkel and A. J. C. Ladd, J. Chem. Phys. **81**, 3188 (1984).
[68] R. Freitas, M. Asta, and M. de Koning, Comput. Mater. Sci. **112**, 333 (2016).
[69] Z. Li, J. R. Kermode, and A. De Vita, Phys. Rev. Lett. **114**, 096405 (2015).
[70] S. Plimpton, J. Comput. Phys. **117**, 1 (1995).
[71] A. R. Oganov, J. Chen, C. Gatti, Y. Y. Ma, Y. Y. Ma, C. W. Glass, Z. Liu, T. Yu, O. O. Kurakevych, and V. L. Solozhenko, Nature (London) **457**, 863 (2009).
[72] Y. Ma, M. Eremets, A. R. Oganov, Y. Xie, I. Trojan, S. Medvedev, A. O. Lyakhov, M. Valle, and V. Prakapenka, Nature (London) **458**, 182 (2009).
[73] W. Zhang, A. R. Oganov, A. F. Goncharov, Q. Zhu, S. E. Boulfelfel, A. O. Lyakhov, E. Stavrou, M. Somayazulu, V. B. Prakapenka, and Z. Konôpková, Science **342**, 1502 (2013).
[74] X. Dong, A. R. Oganov, A. F. Goncharov, E. Stavrou, S. Lobanov, G. Saleh, G.-R. Qian, Q. Zhu, C. Gatti, V. L. Deringer, R. Dronskowski, X.-F. Zhou, V. B. Prakapenka, Z. Konôpková, I. A. Popov, A. I. Boldyrev, and H.-T. Wang, Nat. Chem. **9**, 440 (2017).
[75] S. V. Lepeshkin, V. S. Baturin, Y. A. Uspenskii, and A. R. Oganov, J. Phys. Chem. Lett. **10**, 102 (2019).
[76] See Supplemental Material at http://link.aps.org/supplemental/10.1103/PhysRevB.100.174104 for a description of uranium crystal structures and more detailed uranium *P-T* phase diagrams.
[77] N. D. Mermin, Phys. Rev. **137**, A1441 (1965).
[78] L. D. Landau and E. M. Lifshitz, Course Theor. Phys. **3**, 134 (1994).
[79] J. A. Moriarty, D. A. Young, and M. Ross, Phys. Rev. B **30**, 578 (1984).
[80] M. P. Desjarlais, Phys. Rev. E **88**, 062145 (2013).
[81] V. V. Kechin, Phys. Rev. B **65**, 052102 (2001).